Optik - International Journal for Light and Electron Optics 231 (2021) 166413

Contents lists available at ScienceDirect

Optik

journal homepage: www.elsevier.com/locate/ijleo

Original research article

Optimum weighted multimodal medical image fusion using particle swarm optimization

Shaik Shehanaz, Ebenezer Daniel *, Sitaramanjaneya Reddy Guntur, Sivaji Satrasupalli

Department of Electronics and Communication Engineering, Vignan's Foundation for Science, Technology and Research, Guntur, Andhra Pradesh, 522213, India

ARTICLE INFO

Keywords:
Discrete wavelet transform
Weighted average fusion
Particle swarm optimization
Multimodal image fusion
Medical imaging

ABSTRACT

Medical image fusion is a technique that maps information from multiple image modalities into a single image. In past, several multimodal fusion approaches were developed by various researchers, even so, adaptive fusion and robustness are challenging tasks in clinical diagnosis. In this paper, we developed an optimum weighted average fusion (OWAF) for multimodal medical image fusion to improve the multimodal mapping performance. In our approach, conventional discrete wavelet transform (DWT) is used for the decomposition of input multiple modalities into various subgroups. The resultant energy bands were weighted using optimum weights, attained using well known particle swarm optimization algorithm (PSO). Our proposed approach was tested over MRI-SPECT, MRI-PET and MRI-CT image fusion and we used 20 sets of MR/SPECT, 20 sets of MR/PET and 18 sets of MR/CT for our method validation. The quantitative evaluation were performed using established fusion performance metrics such as structural similarity index measure (SSIM), root mean square error (RMSE), peak signal to noise ratio (PSNR), entropy, mutual information (MI), and Edge-based similarity metric($Q^{AB/F}$). Robustness of our proposed fusion approach is tested over gaussian and speckle noise in all the input modalities. The computational performance of our OAWF with PSO algorithm is tested in terms of computational time. The OWAF showed superior performance than existing conventional fusion approaches in terms of information mapping, edge quality and structural similarity in MR/PET, MR/SPECT and MR/CT images in both normal and noisy fusion backgrounds.

1. Introduction

Image fusion is a well-known technique in image processing, which is used to integrate two or more image data into a single frame [1,2]. Multi modal medical image fusion technique is a robust approach in clinical diagnosis and treatment planning. Multimodal fusion can combine the images obtained from various modalities into a single image [3,4]. The fusion approaches are generally used to map functional image into a structural image in clinical applications [5]. In the past, various imaging modalities, such as magnetic resonance imaging (MRI), computed tomography (CT), positron emission tomography (PET) and single-photon emission computed tomography (SPECT) imaging techniques were used for structural and functional image fusion [5–9].

Previously used well-known spatial transformation techniques are discrete cosine transform (DCT) [10–12], Fast Fourier Transform

* Corresponding author.
E-mail address: ebydaniel89@gmail.com (E. Daniel).

https://doi.org/10.1016/j.ijleo.2021.166413
Received 21 December 2020; Accepted 27 January 2021
Available online 2 February 2021

(FFT) [13–15]and multi-level decomposition technique such as discrete wavelet transform (DWT) [16–20].The various transform-based techniques were used in the past for efficient multimodal fusion applications. Fuzzy transform (FTR) were used for medical image fusion for MR/PET, MR-T1/MR-T2, MR/CT, MR/SPECT and CT/PET image fusion were performed for structural and functional image fusion [21]. In which, they performed FTR based decomposition, and maximum fusion rule was used for anatomical and structural fusion. Manchanda et al., tested the robustness of the FTR fusion technique with zoom noisy medical images. Lifting scheme based biorthogonal wavelet-based transform technique based medical image fusion technique is used to fuse MR and CT images, MR-T1 image and magnetic resonance angiography (MRA) image fusion were analyzed [22].

Multiscale decomposition-based techniques were used for various multimodal medical image fusion applications [23]. Recently Maqsood et al., proposed a two-scale decomposition and sparse representation based fusion technique for MR and CT images. In two-scale decomposition technique, they proposed two layers, such as base layer and detail layers for CT and MR images, respectively [24]. Non-subsampled shearlet transform (NSST) and simplified pulse coupled neural networks (S-PCNNs) based fusion technique is proposed to fuse MR, CT and PET images into a single image frame [25]. In which, PET images were decomposed into hue-saturation-value (HSV) colour space and CT and MR images were decomposed into low and high-frequency coefficients. In discrete ripplet transform-based multi modal medical image fusion input MR and CT images decompose into low frequency and high-frequency sub bands. The CT images were fused using low-frequency fusion rule an, whereas MR images used high-frequency fusion rule and performed ripplet coefficient-based fusion is performed [26]. Hoseny et al., proposed a Dual-Tree Complex Wavelet Transform (DT-CWT) based medical image fusion technique, in which they used approximation coefficient fusion and detail coefficient fusion for complementary image fusion. The DT-CWT technique provided grater gain than various conventional histogram techniques. However, they did not include metabolic imaging such as PET and SPECT modalities; also the robustness test was not performed for noise-free fusion [27]. Padmavathi et al., proposed a decomposed texture based fusion technique for MR/PET image fusion. In which, they used total variation (TV-L1) fusion method. The IHS transferred PET images and spatial domain MR images were decomposed using TV-L1. The particle swarm optimization (PSO) based weight selection is used to texture selection and tested with 23 pairs of MR/PET image datasets [28]. Jiang et al., proposed a laplacian based decomposition for medical image fusion, in which low-frequency image was decomposed and then sparse coefficients were fused in complimentary images. Whereas the high-frequency image were decomposed using weighted least squares (WLS) filter [29]. Although in jiang study, they tested with MR/CT images, whereas they did not test with MR/PET, MR/SPECT image fusion techniques. The conventional image fusion methods have limitations with fusion artifacts [30,31]. In the past, various contrast enhancement methods were implemented for medical image fusion [32], however, the robustness with various input noises was not addressed well. Artifacts and noises are the main challenges in structural and functional image fusion. The objective of our proposed work was to develop a multi-level decomposition technique for structural and metabolic image fusion without artifacts and noise in the fused image.

The rest of the sections are organized as follows; Section 2 presents methods, Section 3 discusses proposed optimum weighted average fusion using PSO in detail, Section 4 presents experimental results and discussion and Section 5 with the conclusion.

2. Methods

2.1. Discrete wavelet transform based decomposition

DWT is a mostly used image decomposition technique in multi modal medical image fusion. DWT decomposes an image without any gap or overlap, and it recovers the original image with the minimal loss. DWT can divide the image into multiple sub bands with a combination of low and high pass filter. Sub bands such as LL (low, low) contains the approximate coefficients LH (low, high), HL (high, low) and HH (high, high) contain the detailed vertical, horizontal and diagonal coefficients respectively [2]. In the second level of decomposition, the LL band can further be divided into four parts. In this way, if an "l" level decomposition is applied on an image, it represented by $3l+1$ sub-band among them LL_l is approximate coefficient band generated by final decomposition level remaining LH_n , HL_n *and* HH_n represents detail coefficients where n = 1,2…l-1 [15].

2.2. Need for weight optimization in multi-level decomposition

Multi-level decomposition provides the approximate and detailed components of the input image. The fusion rules such as average or max fusion are generally used to fuse the coefficients of these components. The coefficients of approximate and detailed components of multi modalities may have more considerable variation as they contain complementary information with a unique representation of features. However, conventional methods such as average fusion and max fusion may not give effective complementary fusion, and it may have a chance to get artifacts and information loss from any modality. Weights overcome the above challenges, were used for coefficients selection. Primary weighted average fusion may not provide effective fused image due to affixed weight value for fusion, due to that optimum weight selection can enhance the performance by selecting the effective weights for multi-level decomposition components.

2.3. Particle Swarm Optimization

Eberhart and Kennedy develop Particle Swarm Optimization (PSO) in 1995 [33]. PSO is a well-known population-based optimization technique, inspired by the social behavior of birds and fish. It can solve many optimization problems, like minimizing function value and hyperparameter selection in neural network training [34]. PSO algorithm includes many concepts like swarming theory and

evolutionary computation to set out optima from search space [35]. PSO is initialized to solve a problem with the population of random solutions, which contains the particle position along with a randomized velocity [33]. The particles move in an N-dimensional search space with initialized random positions and velocities. The objective function evaluates each particle. For all particles, fitness value is calculated depending on the position using a fitness function. The current position of a particle is given as the input to the objective function to get the current location fitness value. Each particle position coordinates are updated by the two best fitness values "*pbest*" *and* "*gbest*" tracked for every time step [36]. The "*pbest*" is the best value achieved by each particle, which is calculated for every iteration. The "*gbest*" is the overall best value obtained by all the particles "*pbest*" values in search space until that time step. For every iteration, if the particles current position fitness value is better than the "*pbest*" value then the current position set as "*pbest*" and the position of best fitness value among all is set as "*gbest*" [37].

The position and velocity of each particle is updated by using Eqs. 1 and 2,

$$X_{n+1}^{i} = X_{n}^{i} + V_{n+1}^{i} \tag{1}$$

$$V_{n+1}^{i} = V_{n}^{i} + c_1 r_1 \left(pbest_{n}^{i} - X_{n}^{i}\right) + c_2 r_2 \left(gbest_{n} - X_{n}^{i}\right) \tag{2}$$

X_{n+1}^{i}, X_{n}^{i} are the new and current position values of particle i respectively

V_{n+1}^{i}, V_{n}^{i} are the new and current velocity of particle i respectively

$pbest_{n}^{i}$ is the *pbest* position of particle i at time set n

$gbest_{n}$ is the *gbest* position of the optimizer at time set n

c_1, c_2 are acceleration factor related to *pbest* and *gbest*.

r_1, r_2 are the randomly generated with the range [0,1].

Two different velocity components were used to calculate the velocity of the particle along with the original velocity. They are cognition acceleration and social acceleration components, which are used to adjust velocity according to best positions. The second and third part of Eq. 2 represents the cognition and social acceleration components, respectively. The positions, velocities of all

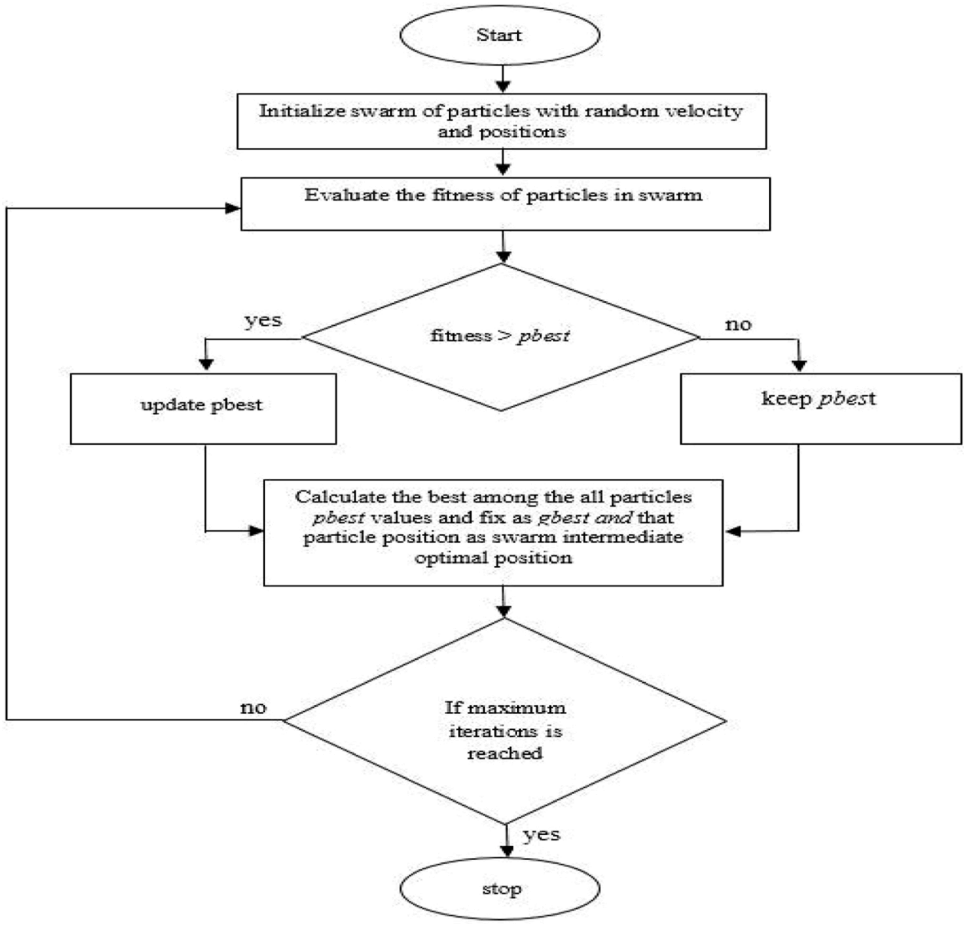

Fig. 1. Flow chart of PSO algorithm.

particles and best values are updated again and again until it reached a pre-determined good fitness [33,37,38]. The flow chart of PSO algorithm is given in Fig. 1.

3. Proposed optimum weighted fusion

The block diagram of proposed OWAF fusion is shown in Fig. 2. In the proposed method, input images are decomposed into approximate and detailed components using discrete wavelet transform (DWT). The approximate and detailed coefficients of the Modality-1 image ($I_{M1}(x,y)$) are in Eqs. (3) and (4) respectively.

$$C_{M1\varphi}(j_o,m,n)=\frac{1}{\sqrt{MN}}\sum_{x=0}^{M-1}\sum_{y=0}^{N-1}I_{M1}(x,y)\varphi(j_o,m,n) \tag{3}$$

$$C_{M1\varphi}^{H_i}(j,m,n)=\frac{1}{\sqrt{MN}}\sum_{x=0}^{M-1}\sum_{y=0}^{N-1}I_{M1}(x,y)\varphi^{H_i}(j,m,n) \tag{4}$$

Similarly, the modality-2 image ($I_{M2}(x,y)$) decomposed coefficients are given in the Eqs. (5) and (6).

$$C_{M2\varphi}(j_o,m,n)=\frac{1}{\sqrt{MN}}\sum_{x=0}^{M-1}\sum_{y=0}^{N-1}I_{M2}(x,y)\varphi \tag{5}$$

$$C_{M2\varphi}^{H_i}(j,m,n)=\frac{1}{\sqrt{MN}}\sum_{x=0}^{M-1}\sum_{y=0}^{N-1}I_{M2}(x,y)\varphi^{H_i}(j,m,n) \tag{6}$$

Where M × N represents the size of input medical image, i = {1,2,3}, C^{H_1}, C^{H_2} and C^{H_3} represents the horizontal, vertical and diagonal components, respectively.

PSO based optimum weight selection was proposed to calculate the optimum weight values for detailed coefficient bands. If w_1, w_2 and w_3 are the optimized weight values for vertical, horizontal and diagonal components, then the range of values can be $0< w_1, w_2, w_3<1$. After proper selection of weight, values the vertical, horizontal and diagonal detailed components are updated and combined with the approximate component. Both modality 1 and modality 2 input image detailed components are given to PSO based optimum weight selection. The calculated optimum weights by PSO are multiplied with the detailed components to generate new detailed components. These modified detailed components are combined with the respective approximate component, they are represented in Eqs. (7) and (8) for modality 1 and modality 2, respectively.

$$C_{M1}^{dwt}=\left\{C_{M1\varphi},\left(w_{M1}^{H_1}*C_{M1\varphi}^{H_1},w_{M1}^{H_2}*C_{M1\varphi}^{H_1},w_{M1}^{H_3}*C_{M1\varphi}^{H_3}\right)\right\} \tag{7}$$

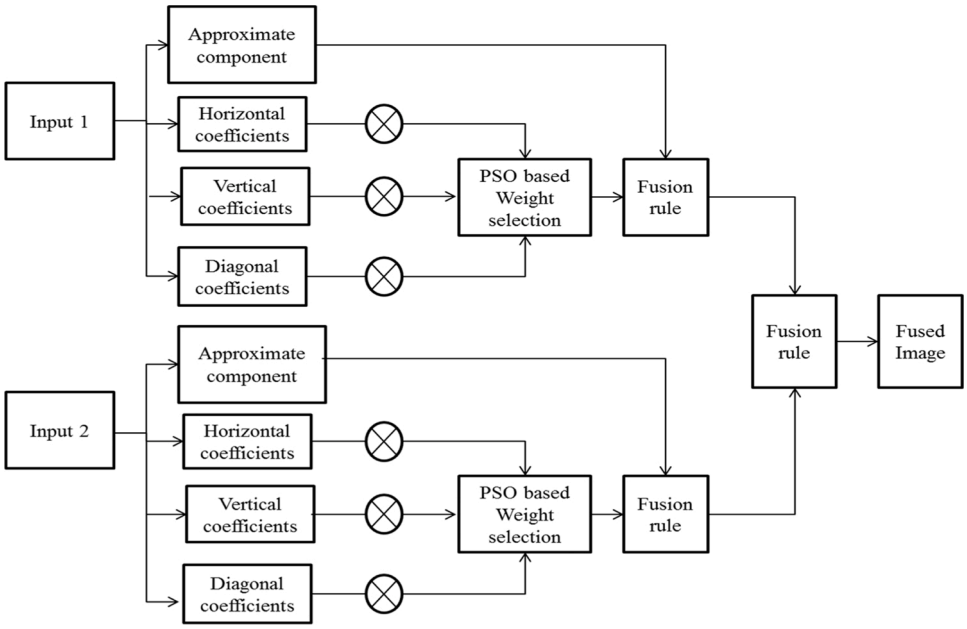

Fig. 2. Proposed optimum weighted average fusion using PSO.

$$C_{M2}^{dwt} = C_{M2\varphi},\ \left\{ \left(w_{M2}^{H_1} * C_{M2\varphi}^{H_1}, w_{M2}^{H_2} * C_{M2\varphi}^{H_2}, w_{M2}^{H_3} * C_{M2\varphi}^{H_3} \right) \right\} \tag{8}$$

The updated coefficient values are fused using average fusion. Inverse wavelet transform is applied to final fused coefficients to generate the final fused image.

$$C_{fused}^{dwt} = \frac{(C_{M1}^{dwt} + C_{M2}^{dwt})}{2} \tag{9}$$

$$I_{fused} = idwt\{C_{fused}^{dwt} \tag{10}$$

4. Experimental results and discussion

To evaluate the performance of the proposed fusion technique multi-modality medical imaging pairs MR-CT, MR-PET and MR-SPECT are considered. The proposed fusion technique, OWAF is compared with standard fusion methods such as SAF, IHS, FFT, and DWT.

The dataset is available in http://www.med.harvard.edu/AANLIB/.

4.1. Quantitative evaluation metrics

Performance evaluation of the fusion method is determined by the quality assessment of the fused image. Automatic performance evolution is still a challenging and essential task in the field of image fusion. Objective quality evaluation is performed using quan-

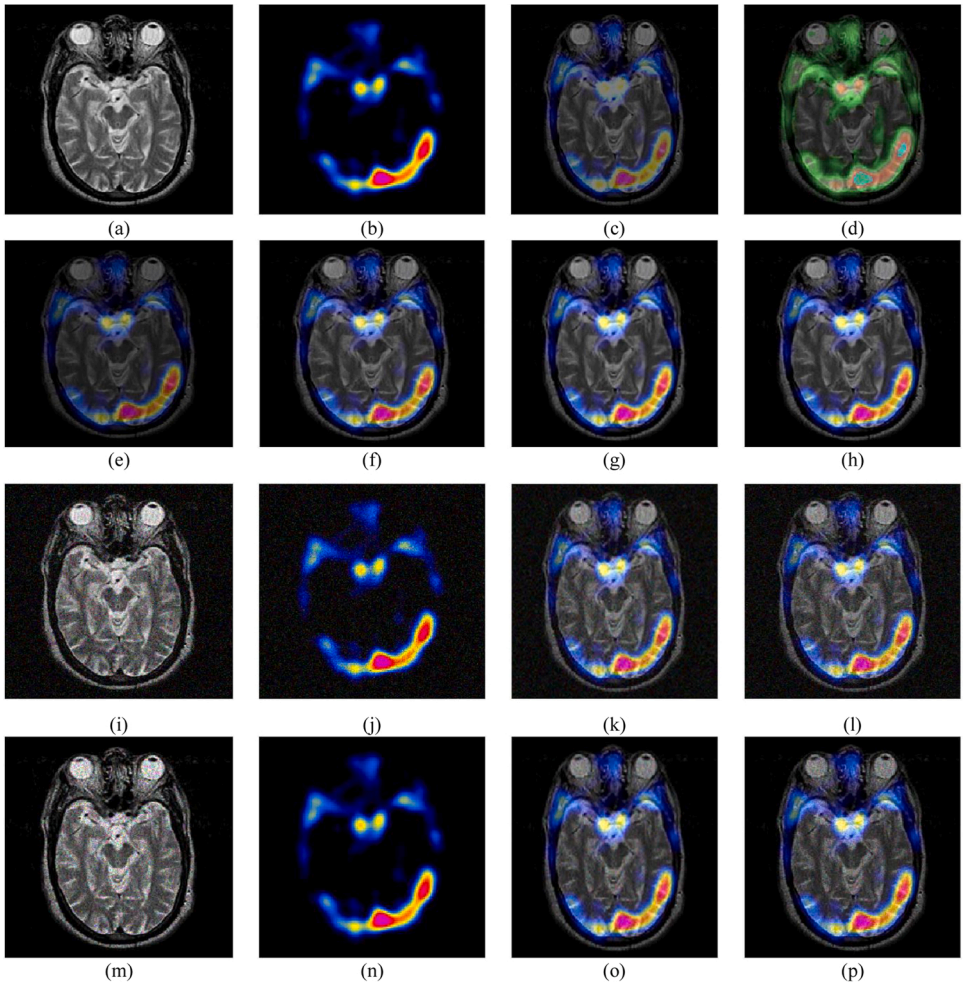

Fig. 3. MR_SPECT fusion result: **(a)** MR **(b)** SPECT **(c)** SAF **(d)** HIS **(e)** FFT **(f)** DWT **(g)** Proposed WAF **(h)** Proposed OWAF with PSO **(i)** noisy MR (gaussian) **(j)** noisy SPECT (gaussian) **(k)** Proposed WAF noisy gaussian **(l)** Proposed OWAF with PSO noisy Gaussian **(m)** noisy MR(speckle) **(n)** noisy SPECT (speckle) **(o)** Proposed WAF noisy speckle **(p)** Proposed OWAF with PSO noisy speckle.

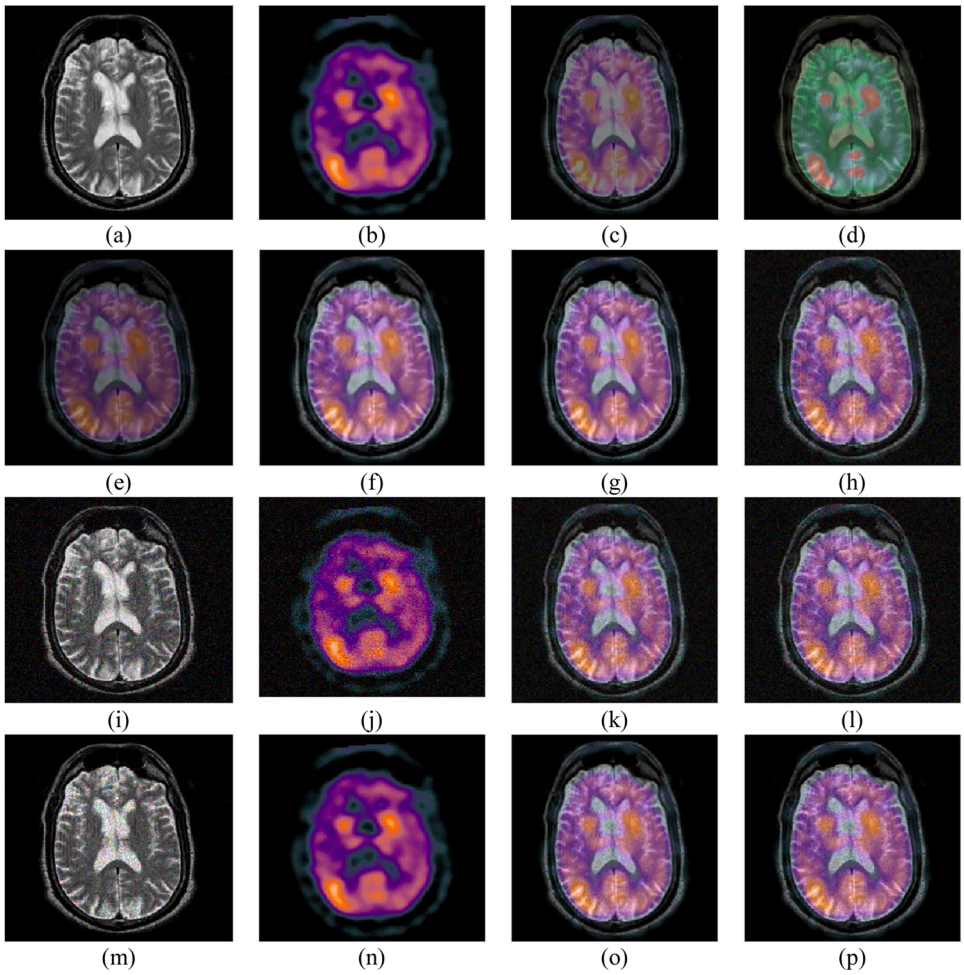

Fig. 4. MR_SPECT fusion result: **(a)** MR **(b)** SPECT **(c)** SAF **(d)** HIS **(e)** FFT **(f)** DWT **(g)** Proposed WAF **(h)** Proposed OWAF with PSO **(i)** noisy MR (gaussian) **(j)** noisy SPECT (gaussian) **(k)** Proposed WAF noisy gaussian **(l)** Proposed OWAF with PSO noisy gaussian **(m)** noisy MR (speckle) **(n)** noisy SPECT (speckle) **(o)** Proposed WAF noisy speckle **(p)** Proposed OWAF with PSO noisy speckle.

titative metrics. Many quantitative metrics have been proposed and are used by researchers for fusion method evaluation. Among which, few metrics such as SSIM [3,12], RMSE [10], PSNR [5] entropy [17], mutual information (MI) [1–5,7], and Edge-based similarity metric $Q^{AB/F}$ [4,2–5] are selected. Wang and Bovik [35] proposed an image quality assessment metric based on structural similarity index measurement. SSIM used to measures luminance, contrast, and structure of image to evaluate the quality of the image and given in Eq. (11).

$$SSIM(I,F) = [l(I,F)]^a.[c(I,F)]^b.[s(I,F)]^c \tag{11}$$

If A and B are input images, then final mean SSIM is calculated using Eq. (12)

$$SSIM = \frac{1}{2}[SSIM(A,F) + SSIM(B,F)\ ] \tag{12}$$

Table 1
Average performance metrics of MR-SPECT image fusion.

Method	SSIM	RMSE	MI	PSNR	$Q^{AB/F}$	Entropy
SAF	0.6390	0.4672	1.5165	22.71	0.5012	3.734
IHS	0.6615	0.4146	1.6722	23.85	0.5405	3.984
FFT	0.6885	0.2864	2.4891	23.34	0.5491	4.145
DWT	0.7915	0.2154	2.5901	29.61	0.6236	4.573
Proposed WAF	0.8491	0.1263	2.8745	31.83	0.8129	4.702
Proposed OWAF-PSO	0.9154	0.0261	3.1652	34.27	0.8653	5.274

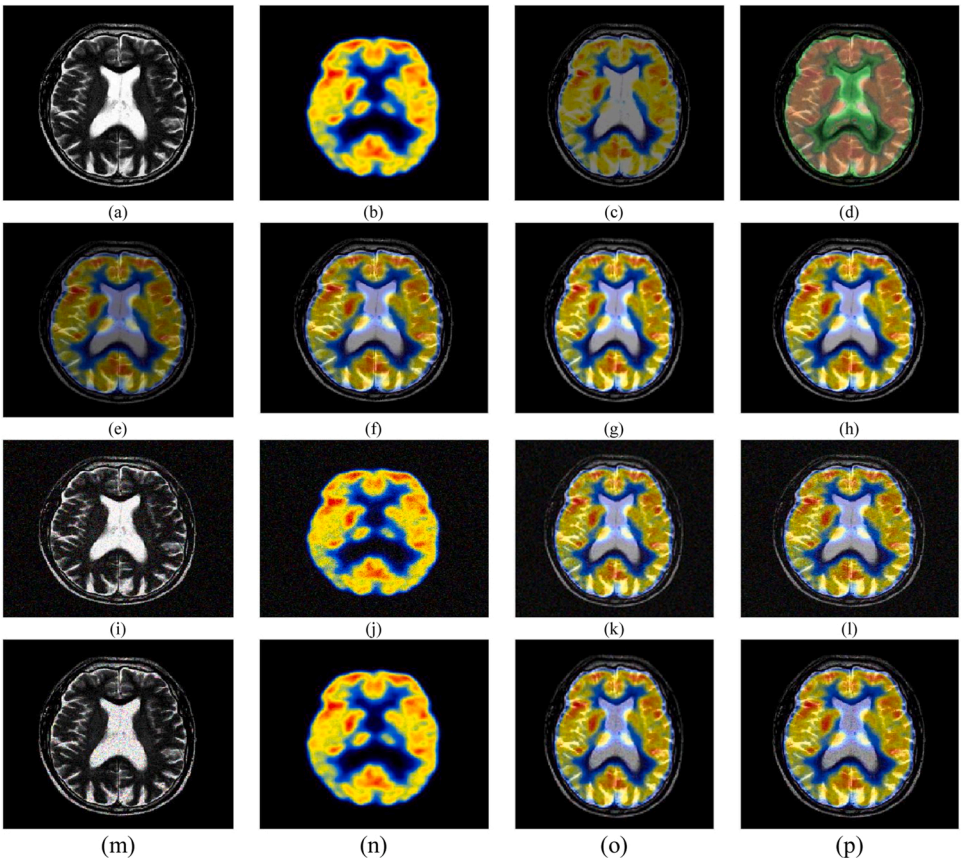

Fig. 5. MR_PET fusion result: **(a)** MR **(b)** PET **(c)** SAF **(d)** HIS **(e)** DCT **(f)** DWT **(g)** Proposed WAF **(h)** Proposed OWAF with PSO **(i)** noisy MR (Gaussian) **(j)** noisy SPECT (Gaussian) **(k)** Proposed WAF noisy gaussian **(l)** Proposed OWAF with PSO noisy Gaussian **(m)** noisy MR (speckle) **(n)** noisy SPECT (speckle) **(o)** Proposed WAF noisy speckle **(p)** Proposed OWAF with PSO noisy speckle.

RMSE is used to measure accuracy in incorporating information from input images. It is calculated by Eq. (13)

$$RMSE = \left(\sum_{x=1}^{M} \sum_{y=1}^{N} [I_A(x,y) + I_B(x,y)]^2 \right)^{1/2} \tag{13}$$

PSNR is an objective quality metric and is calculated by Eq. (14)

$$PSNR = 10.\log\left[(M \times N)^2 / RMSE\right] \tag{14}$$

Mutual information is a quantitative metric used to evaluate the mutual dependency of two images. MI between the fused image and the source image is defined as

$$MI = MI_{AF} + MI_{BF} \tag{15}$$

$$MI_{AF}(a,f) = \sum_{a,f} P_{AF}(a,f) \log_2 \frac{P_{AF}(a,f)}{P_A(a) P_F(f)} \tag{16}$$

$$MI_{BF}(b,f) = \sum_{a,f} P_{BF}(b,f) \log_2 \frac{P_{BF}(b,f)}{P_B(b) P_F(f)} \tag{17}$$

$P_A(a)$, $P_B(b)$, and $P_F(f)$ are the normalized histogram of the source images and the fused image. $P_{BF}(b,f)$, and $P_{BF}(b,f)$ are the joint normalized histograms between the fused image and the source images A and B.

Xydeas and Petrovic [36] proposed Edge-based similarity metric $Q^{AB/F}$ to calculate the amount of edge information transferred from the input image to the fused image. $Q^{AB/F}$ is calculated using Eq. (18).

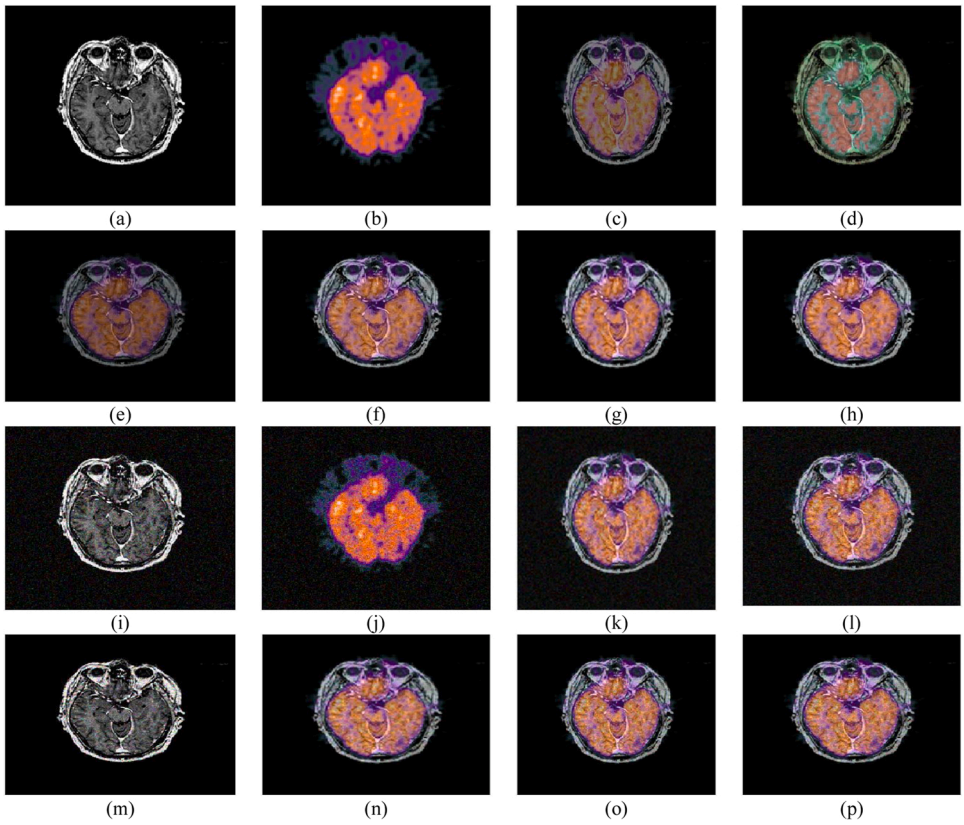

Fig. 6. MR_PET fusion result: **(a)** MR **(b)** PET **(c)** SAF **(d)** HIS **(e)** DCT **(f)** DWT **(g)** Proposed WAF **(h)** Proposed OWAF with PSO **(i)** noisy MR (Gaussian) **(j)**noisy SPECT (Gaussian) **(k)** Proposed WAF noisy gaussian **(l)** Proposed OWAF with PSO noisy Gaussian **(m)** noisy MR (speckle) **(n)** noisy SPECT (speckle) **(o)** Proposed WAF noisy speckle **(p)** Proposed OWAF with PSO noisy speckle.

Table 2
Average performance metrics of MR-PET image fusion.

Method	SSIM	RMSE	MI	PSNR	$Q^{AB/F}$	Entropy
SAF	0.5532	0.8362	1.7031	19.78	0.4841	4.251
IHS	0.5620	0.7743	1.8022	21.41	0.5197	4.326
FFT	0.6126	0.6022	1.9731	24.80	0.5254	4.389
DWT	0.7984	0.3423	2.4270	26.39	0.6743	4.684
Proposed WAF	0.8712	0.1270	3.2651	34.63	0.8380	5.038
Proposed OWAF-PSO	0.9218	0.0345	3.5043	37.82	0.8669	5.387

$$Q^{AB/F} = \frac{\sum_{i=1}^{M}\sum_{j=1}^{N}\left(Q^{A/F}w_A(i,j) + Q^{B/F}w_B(i,j)\right)}{\sum_{i=1}^{M}\sum_{j=1}^{N}\left(w_A(i,j) + w_B(i,j)\right)} \tag{18}$$

Where $Q^{A/F}$ and $Q^{B/F}$ are the edge information preservation values. $w_A(i,j)$, $w_B(i,j)$ are the weights that reflect the importance of $Q^{A/F}$ and $Q^{B/F}$ respectively. If the value of $Q^{AB/F}$ is grater then fused image displays better edge information. Entropy is used to measure image information, where a higher value indicates the grandness (richness) of image information.

$$Entropy = -\sum_{a=0}^{N} p_a \ln p_a \tag{19}$$

Where p_a is the probability distribution of the pixel "a" over other pixels.

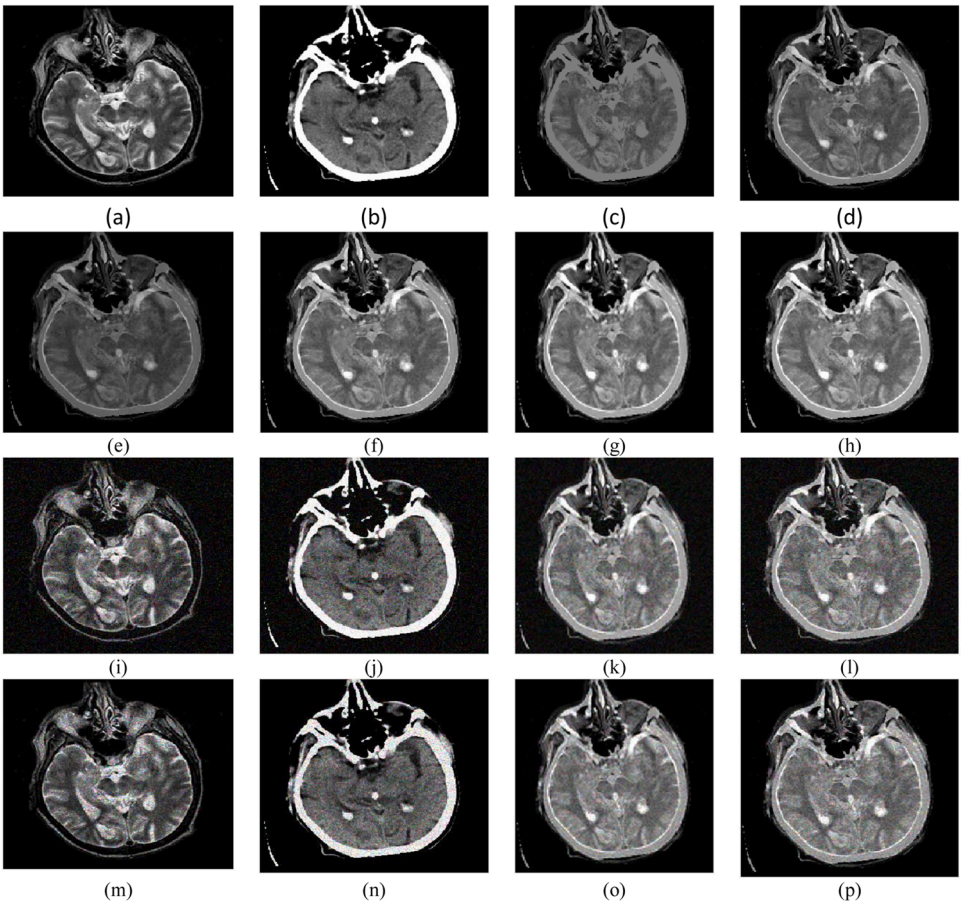

Fig. 7. MR_CT fusion result: **(a)** MR **(b)** CT **(c)** SAF **(d)** HIS **(e)** DCT **(f)** DWT **(g)** Proposed WAF **(h)** Proposed OWAF with PSO **(i)** noisy MR (Gaussian) **(j)** noisy SPECT (Gaussian) **(k)** Proposed WAF noisy gaussian **(l)** Proposed OWAF with PSO noisy Gaussian **(m)** noisy MR (speckle) **(n)** noisy SPECT (speckle) **(o)** Proposed WAF noisy speckle **(k)** Proposed OWAF with PSO noisy speckle.

4.2. MR/SPECT fusion

MR and SPECT image fusion results are shown in Figs. 3 and 4. Fig. 3(a), Fig. 4(a), 3 (b) and 4 (b) are the input MR and SPECT images, respectively. The fused images Fig. 3(c), 4 (c), 3 (e) and 4 (e) are generated by the SAF and FFT based fusion respectively showed the less contrast. Color distortion is observed by IHS based fusion shown in Figs. 3(d) and 4 (d). DWT based fusion is showing less spatial resolution shown in Figs. 3(f) and 4 (f). The proposed OWAF with PSO results in a better fused image Figs. 3(h) and 4 (h) on comparing with proposed WAF (see Fig. 3(g)) and other methods. The metrics values showed that the proposed technique provides better quantitative results in terms of SSIM, MI, RMSE, PSNR, $Q^{AB/F}$ and entropy. The average quality metrics for the 20 pairs of MR-SPECT images are listed in Table 1. The comparative analysis of the metrics for all methods have showed better performance. The proposed OWAF achieved higher metrics values nearly 7.2 %, 9.2 %, 7.1 %, 6.05 % and 10.8 % improvement in SSIM, MI, PSNR, $Q^{AB/F}$ and entropy values, when compared with best values of existing methods and WAF.

4.3. MR/PET fusion

MR and PET image fusion results are shown in Figs. 5 and 6. The Figs. 5(a), 6 (a), 5 (b) and 6 (b) represents the input MR and PET images respectively and 5 (c) -5 (h) and 6 (c) – 6 (h) are represents fused result obtained by SAF, IHS, FFT, DWT, WAF and proposed OWAF. The SAF method Figs. 5(c) and 6 (c) provided spatial distortion due to improper integration of information. Color distortion is also observed in the case of MR-PET image fusion by HIS shown in Fig. 5(d) and 6 (d). The results showed that the proposed OWAF is better in terms of contrast and integrating the metabolic information in comparison with other methods. The average quality metrics for the 20 pairs of MR-PET images are listed in Table 2. The comparative analysis of the metrics for all methods has drawn some important points, are useful to evaluate the performance of fusion methods. The proposed OWAF achieves higher metrics values nearly 5.48 %, 6.82 %, 8.43 %, 3.33 %, and 6.48 % improvement in SSIM, MI, PSNR, $Q^{AB/F}$ and entropy values when compared with best values of existing methods proposed WAF method.

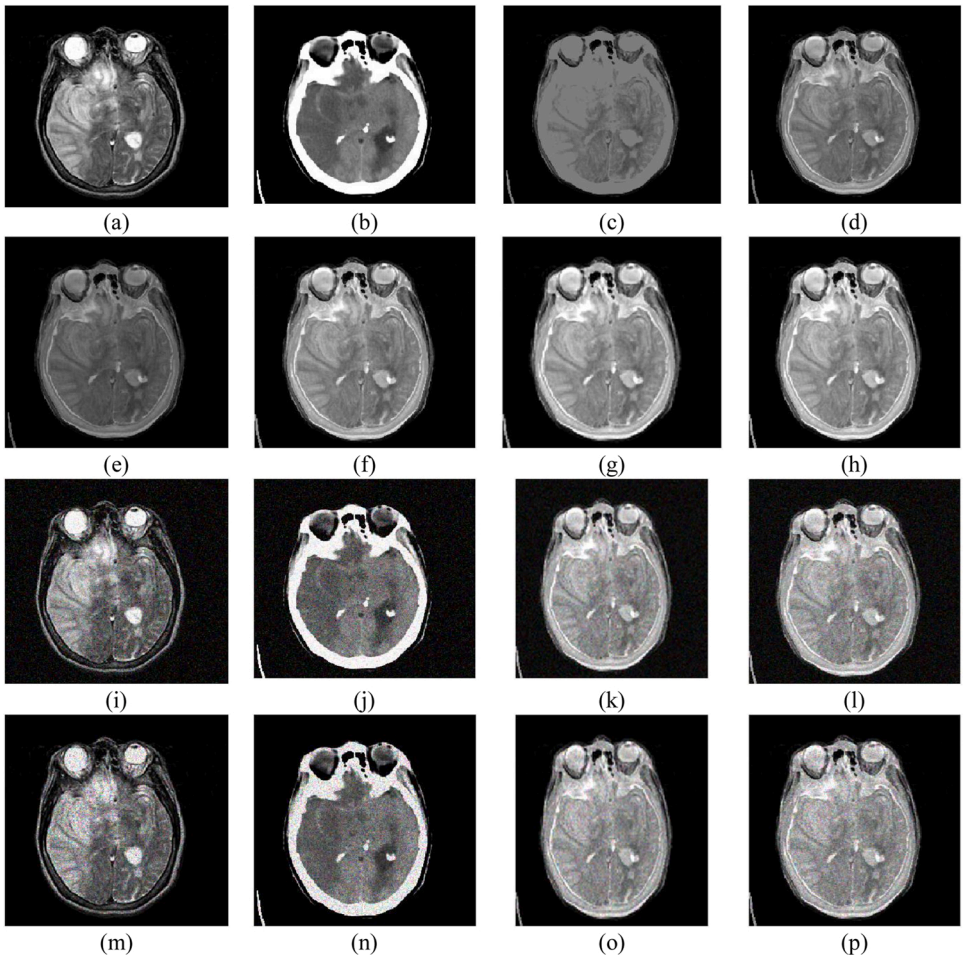

Fig. 8. MR_CT fusion result: **(a)** MR **(b)** CT **(c)** SAF **(d)** HIS **(e)** DCT **(f)** DWT **(g)** Proposed WAF **(h)** Proposed OWAF with PSO **(i)**noisy MR (Gaussian) **(j)** noisy SPECT (Gaussian) **(k)** Proposed WAF noisy gaussian **(l)** Proposed OWAF with PSO noisy Gaussian **(m)** noisy MR (speckle) **(n)** noisy SPECT (speckle) **(o)** Proposed WAF noisy speckle **(p)** Proposed OWAF with PSO noisy speckle.

Table 3
Average performance metrics of MR-CT image fusion.

Method	SSIM	RMSE	MI	PSNR	$Q^{AB/F}$	Entropy
SAF	0.6287	0.9432	1.8071	20.13	0.4243	4.087
IHS	0.6408	0.8904	1.8832	23.87	0.4675	4.231
FFT	0.6783	0.6143	2.1427	24.46	0.4987	4.498
DWT	0.7601	0.4507	2.8650	28.98	0.6208	4.621
Proposed WAF	0.8463	0.1875	3.4379	32.67	0.8546	5.012
Proposed OWAF-PSO	0.9457	0.0832	3.7865	35.65	0.8781	5.3014

Table 4
Performance metrics of image fusion for robustness check.

Modalities	Noise	SSIM	RMSE	MI	PSNR	$Q^{AB/F}$	Entropy
MR-SPECT		0.8843	0.0216	3.0141	26.43	0.6782	4.672
MR-PET	**Gaussian Noise**	0.8521	0.0761	3.2315	28.09	0.7561	4.887
MR-CT		0.8762	0.2076	2.9023	27.86	0.7209	4.843
MR-SPECT		0.9022	0.0350	3.0682	30.04	0.7645	5.012
MR-PET	**Speckle Noise**	0.9276	0.0603	3.4211	30.23	0.7950	5.154
MR-CT		0.9387	0.1251	3.3902	30.08	0.8113	5.024

Table 5
Computational analysis of PSO.

Multimodal approach	Optimum weight values (PSO)		Computational time (seconds)	
	w 1	w2	OWAF-GA	OWAF-PSO
MR-SPECT	0.6287	0.9432	608.14	312.23
MR-PET	0.6408	0.8904	589.43	305.46
MR_CT	0.6783	0.6143	645.42	296.54

4.4. MR/CT fusion

MR and CT image fusion results are shown in Figs. 7 and 8, Fig. 7(a), Fig. 8(a), Fig. 7(b) and 8 (b) represents the input MR and CT images respectively. Fig. 7(c)–(h), Fig. 8(c)–(h) are represents fused result obtained by SAF, IHS, FFT, DWT, WAF and proposed OWAF. Information loss is observed by SAF method shown in Figs. 7(c) and 8 (c). The result obtained by IHS integrated the contour component of the CT with MR in better way on comparison with result obtained by FFT, however both generated contrast restricted images. Contour component of CT image integration with MR is better in IHS based fusion on comparison with FFT based fusion. The contrast of image is less show in Figs. 7(d) and 8 (d) are results of IHS based fusion. The results showed that the proposed OWAF is better in terms of contrast and structural detailing in comparison with other methods. The metrics values shows that proposed technique provided better quantitative results in terms of SSIM, MI, RMSE, PSNR, $Q^{AB/F}$ and entropy. The average quality metrics for the 18 pairs of MR-CT images are listed in Table 3.

The proposed OWAF achieves higher metrics values nearly 10.5 %, 9.2 %, 8.3 %, 2.6 %, and 5.4 % improvement in SSIM, MI, PSNR, $Q^{AB/F}$ and entropy values when compared with best values of existing methods proposed WAF method.

4.5. Robustness analysis

The robustness of the proposed techniques is evaluated with the help of corrupted images generated by adding noise manually. Gaussian noise added MR and SPECT images (Fig. 3(i), Fig. 4(i), Fig. 3(j) and Fig. 4(j) respectively) are given as input to proposed techniques. The fused image using WAF and proposed OWAF with PSO is shown in Fig. 3(k), Fig. 4(k), Fig. 3(l) and Fig. 4(l) respectively. The speckle noise added MR and SPECT images (Fig. 3(m), Fig. 4(m), Fig. 3(n) and Fig. 4(n) respectively) are given as input to proposed techniques. The fused image using WAF and proposed OWAF with PSO is shown in Fig. 3(o), Fig. 4(o), Fig. 3(p) and Fig. 4(p) respectively. The gaussian noise added MR and PET images (Fig. 5(i), Fig. 6(i), Fig. 5(j) and Fig. 6(j) respectively) are given as input to proposed techniques. The fused image using WAF and proposed OWAF with PSO is shown in Fig. 5(k), Fig. 6(k), Fig. 5(l) and Fig. 6(l) respectively. The speckle noise added MR and SPECT images (Fig. 5(m), Fig. 6(m), Fig. 5(n) and Fig. 6(n) respectively) are given as input to proposed techniques. The fused image using WAF and proposed OWAF with PSO is shown in Fig. 5(o), Fig. 6(o), Fig. 5 (p) and Fig. 6(p) respectively. The gaussian noise added MR and CT images (Fig. 7(i), Fig. 8(i), Fig. 7(j) and Fig. 8(j) respectively) are given as input to proposed techniques. The fused image using WAF and proposed OWAF with PSO is shown in Fig. 7(k), Fig. 8(k), Fig. 7 (l) and Fig. 8(l) respectively. The speckle noise added MR and SPECT images (Fig. 7 (m), Fig. 8(m), Fig. 7(n) and Fig. 8(n) respectively) are given as input to proposed techniques. The fused image using WAF and proposed OWAF with PSO is shown in Fig. 7(o), Fig. 8(o), Fig. 7(p) and Fig. 8(p) respectively. The quantitative analysis of robustness check is given in Table 4. The quantitative results showed that our proposed OWAF technique has grater withstanding with noisy background.

4.6. Implementation results of PSO algorithm

The optimum weight values of our proposed OAWF technique is obtained using PSO algorithm. The weight values populations are randomly generated with number of populations is 50. We have used, 50 iterations (fixed using trial and error method) for the selection of optimum weight values. The computational complexity is compared with well-known Genetic Algorithm (GA) in terms of computational time (seconds) and given in Table 5. The computational time showed that PSO algorithm has better computational performance in terms of computational time.

5. Conclusion

In this paper, we proposed an OWAF method using PSO for multimodal brain image fusion. The proposed OWAF showed higher results over the state-of-the-art fusion methods in quantitative and qualitative evaluation. The quantitative evaluation is performed based on standard fusion quality metrics such as SSIM, MI, PSNR, RMSE, $Q^{AB/F}$ and Entropy. The quantitative analysis effectively evaluated the quality of fusion in terms of signal quantity, error rate, edge strength and retained information. Our OWAF, showed higher performance in terms of all six evaluated measures, in comparison with well known existing techniques. Also, we have tested the robustness of OWAF with gaussian and speckle noisy background. Robustness check results showed that, our approach can withstand with general noisy background. The computational complexity with optimization algorithm is measured using computational time in seconds, however our OWAF with PSO significantly reduced the computational time than conventional GA approach. The limitations of our method also noted here. In this approach, we used normalized and registered public image dataset, however in

future we need to further develop registration algorithms for the purpose of multicentral applications. Also, recently various new optimization algorithms developed by various researchers, in future hybrid approaches may able to reduce further computational time

Declaration of Competing Interest

The authors report no declarations of interest.

References

[1] H.T. Mustafa, J. Yang, H. Mustafa, M. Zareapoor, Infrared and visible image fusion based on dilated residual attention network, Optik 224 (2020) p. 165409, 2020/12/01.
[2] H. Yan, Z. Li, Infrared and visual image fusion based on multi-scale feature decomposition, Optik 203 (2020) 163900, 2020/02/01.
[3] S.M. Darwish, Multi-level fuzzy contourlet-based image fusion for medical applications, IET Image Process. 7 (7) (2013) 694–700.
[4] J. Du, W. Li, K. Lu, B. Xiao, An overview of multi-modal medical image fusion, Neurocomputing 215 (2016) 3–20, 2016/11/26.
[5] L. Wang, B. Li, L.-f. Tian, Multi-modal medical image fusion using the inter-scale and intra-scale dependencies between image shift-invariant shearlet coefficients, Inf. Fusion 19 (2014) 20–28, 2014/09/01.
[6] E. Daniel, Optimum wavelet-based homomorphic medical image fusion using hybrid genetic–Grey Wolf optimization algorithm, IEEE Sens. J. 18 (16) (2018) 6804–6811.
[7] E. Daniel, J. Anitha, J. Gnanaraj, Optimum laplacian wavelet mask based medical image using hybrid cuckoo search – grey wolf optimization algorithm, Knowledge Based Syst. 131 (2017) 58–69, 2017/09/01.
[8] X. Liu, W. Mei, H. Du, Multi-modality medical image fusion based on image decomposition framework and nonsubsampled shearlet transform, Biomed. Signal Process. Control 40 (2018) 343–350, 2018/02/01.
[9] M. Haribabu, V. Guruvaiah, Statistical measurements of multi modal MRI – PET medical image fusion using 2D – HT in HSV color space, Procedia Comput. Sci. 165 (2019) 209–215, 2019/01/01.
[10] U.R. Acharya, et al., An integrated index for identification of fatty liver disease using radon transform and discrete cosine transform features in ultrasound images, Inf. Fusion 31 (2016) 43–53, 2016/09/01.
[11] Y.A.V. Phamila, R. Amutha, Discrete Cosine Transform based fusion of multi-focus images for visual sensor networks, Signal Processing 95 (2014) 161–170, 2014/02/01.
[12] P. Ravi, J. Krishnan, Image Enhancement with Medical Image Fusion using Multiresolution Discrete Cosine Transform, Mater. Today Proc. 5 (1, Part 1) (2018) 1936–1942, 2018/01/01.
[13] L. Chang, X. Feng, X. Li, R. Zhang, A fusion estimation method based on fractional Fourier transform, Digit. Signal Process. 59 (2016) 66–75, 2016/12/01.
[14] G. Palanikumar, S. Shanmugan, V. Chithambaram, Solar cooking thermal image processing applied to time series analysis of fuzzy stage and inconsiderable Fourier transform method, Mater. Today Proc. (2020), 2020/03/28.
[15] J.B. Sharma, K.K. Sharma, V. Sahula, Hybrid image fusion scheme using self-fractional Fourier functions and multivariate empirical mode decomposition, Signal Process. 100 (2014) 146–159, 2014/07/01.
[16] V. Bhavana, H.K. Krishnappa, Multi-modality medical image fusion using discrete wavelet transform, Procedia Comput. Sci. 70 (2015) 625–631, 2015/01/01.
[17] C.T. Kavitha, C. Chellamuthu, R. Rajesh, Medical image fusion using combined discrete wavelet and ripplet transforms, Procedia Eng. 38 (2012) 813–820, 2012/01/01.
[18] O. Prakash, C.M. Park, A. Khare, M. Jeon, J. Gwak, Multiscale fusion of multimodal medical images using lifting scheme based biorthogonal wavelet transform, Optik 182 (2019) 995–1014, 2019/04/01.
[19] R. Vijayarajan, S. Muttan, Discrete wavelet transform based principal component averaging fusion for medical images, AEU - Int. J. Electron. Commun. 69 (6) (2015) 896–902, 2015/06/01.
[20] S. Polinati, R. Dhuli, Multimodal medical image fusion using empirical wavelet decomposition and local energy maxima, Optik 205 (2020) 163947, 2020/03/01.
[21] M. Manchanda, R. Sharma, A novel method of multimodal medical image fusion using fuzzy transform, J. Vis. Commun. Image Represent. 40 (2016) 197–217, 2016/10/01.
[22] N. Paramanandham, K. Rajendiran, Infrared and visible image fusion using discrete cosine transform and swarm intelligence for surveillance applications, Infrared Phys. Technol. 88 (2018) 13–22, 2018/01/01.
[23] R.R. Nair, T. Singh, An Optimal Registration on Shearlet domain with Novel Weighted Energy fusion for Multi-Modal Medical Images, Optik 225 (2021) 165742, 2021/01/01.
[24] S. Maqsood, U. Javed, Multi-modal medical image fusion based on two-scale image decomposition and sparse representation, Biomed. Signal Process. Control 57 (2020) 101810, 2020/03/01.
[25] X. Jin, G. Chen, J. Hou, Q. Jiang, D. Zhou, S. Yao, Multimodal sensor medical image fusion based on nonsubsampled shearlet transform and S-PCNNs in HSV space, Signal Processing 153 (2018) 379–395, 2018/12/01.
[26] S. Singh, R.S. Anand, Ripplet domain fusion approach for CT and MR medical image information, Biomed. Signal Process. Control 46 (2018) 281–292, 2018/09/01.
[27] H.M. El-Hoseny, W. Abd El-Rahman, E.-S.M. El-Rabaie, F.E. Abd El-Samie, O.S. Faragallah, An efficient DT-CWT medical image fusion system based on modified central force optimization and histogram matching, Infrared Phys. Technol. 94 (2018) 223–231, 2018/11/01.
[28] K. Padmavathi, C.S. Asha, V.K. Maya, A novel medical image fusion by combining TV-L1 decomposed textures based on adaptive weighting scheme, Eng. Sci. Technol. Int. J. 23 (1) (2020) 225–239, 2020/02/01.
[29] W. Jiang, et al., Medical images fusion by using weighted least squares filter and sparse representation, Comput. Electr. Eng. 67 (2018) 252–266, 2018/04/01.
[30] H. Chen, Fusion denoising algorithm of optical coherence tomography image based on point-estimated and block-estimated, Optik 225 (2021) 165864, 2021/01/01.
[31] M. Park, et al., Deep learning-based noise reduction algorithm using patch group technique in cadmium zinc telluride fusion imaging system: a Monte Carlo simulation study, Optik 207 (2020) 164472, 2020/04/01.
[32] E. Daniel, J. Anitha, K.K. Kamaleshwaran, I. Rani, Optimum spectrum mask based medical image fusion using Gray Wolf Optimization, Biomed. Signal Process. Control 34 (2017) 36–43, 2017/04/01.
[33] R. Eberhart, J. Kennedy, A new optimizer using particle swarm theory, MHS'95. Proceedings of the Sixth International Symposium on Micro Machine and Human Science (1995) 39–43.
[34] Fvd. Bergh, A.P. Engelbrecht, A Cooperative approach to particle swarm optimization, IEEE Trans. Evol. Comput. 8 (3) (2004) 225–239.
[35] Z. Cui, X. Gao, Theory and applications of swarm intelligence, Neural Comput. Appl. 21 (2) (2012) 205–206, 2012/03/01.
[36] Z. Xiaoqin, H. Weiming, S. Maybank, L. Xi, Z. Mingliang, Sequential particle swarm optimization for visual tracking, 2008 IEEE Conference on Computer Vision and Pattern Recognition (2008) 1–8.
[37] A. Tharwat, M. Elhoseny, A.E. Hassanien, T. Gabel, A. Kumar, Intelligent bézier curve-based path planning model using chaotic particle swarm optimization algorithm, Cluster Comput. 22 (2) (2019) 4745–4766, 2019/03/01.
[38] K.R. Harrison, A.P. Engelbrecht, B.M. Ombuki-Berman, Self-adaptive particle swarm optimization: a review and analysis of convergence, Swarm Intell. 12 (3) (2018) 187–226, 2018/09/01.